EUROPEAN ORGANIZATION FOR NUCLEAR RESEARCH

CERN/EP 87-113 Rev.
12 February, 1988

# TWO-PARTICLE CORRELATIONS IN 360 GeV/c pp INTERACTIONS

NA23, EHS – RCBC Collaboration

Bombay[1], Budapest[2], CERN[3], Chandigarh[4], Genova[5], Innsbruck[6], Japan-UG[7], Madrid[8], Mons[9], Moscow[10], Serpukhov[11], Vienna[12] Collaboration

J.L. Bailly[9], S. Banerjee[1], F. Bruyant[3], B. Buschbeck[12], C. Caso[5], H. Dibon[12], B. Epp[6], A. Ferrando[8], F. Fontanelli[5], T. Gemesy[2], A. Gurtu[1], R. Hamatsu[7a], Ph. Herquet[9], T. Hirose[7a], , J. Hrubec[12], Yu. Ivanysherkov[11], E.P. Kistenev[11], N. Khalatyan[11], S. Kitamura[7a], T. Kreuzberger[12], V. Kubik[11], P. Lipa[12], J. MacNaughton[12], P.K. Malhotra[1], M. Markytan[12], I.S. Mittra[4], L. Montanet[3], G. Neuhofer[3], G. Pinter[2], P. Porth[12], R. Raghavan[1], T. Rodrigo[8], J.B. Singh[4], S. Squarcia[5], U. Trevisan[5], K. Takahashi[7b], L.A. Tikhonova[10], T. Yamagata[7a], G. Zholobov[11], J. Zoll[3] and S.A. Zotkin[10]

## Abstract

Two particle correlations of hadrons produced in 360 GeV/c pp interactions are investigated in the transverse plane and in rapidity. The data were obtained at the European Hybrid Spectrometer equipped with a Rapid Cycling Bubble Chamber. The observed transverse and rapidity correlations are compared with the one string LUND- and a two string Dual Parton-model. These models predict in general stronger correlations in the transverse plane and much weaker correlations in rapidity than found in the data. The LUND-FRITIOF- and Multichain Dual Parton Models provide a better reproduction of the data, although the agreement is not yet satisfactory. Only the UA5 cluster model GENCL shows agreement with the data.

Submitted to Zeitschrift für Physik C

1 Tata Institute of Fundamental Research, 400005 Bombay, India

2 Central Research Institute for Physics, H-1525 Budapest 114, Hungary

3 CERN, European Organization for Nuclear Research, CH-1211 Geneva 23, Switzerland

4 Panjab University, 160014 Chandigarh, India

5 University of Genova and INFN, I-16146 Genova, Italy

6 Institut für Experimentalphysik, University of Innsbruck, A-6020 Innsbruck, Austria *)

7a Tokyo Metropolitan University, 158 Tokyo, Japan

7b Tokyo University of Agriculture and Technology, Tokyo, Japan

7c Chuo University, Tokyo, Japan

7d Hiroshima University, 730 Hiroshima, Japan

8 Junta de Energia Nuclear, Madrid 3, Spain

9 Université de l'Etat, Faculté des Sciences, B-7000 Mons, Belgium

10 Moscow State University, SU-117234 Moscow, USSR

11 Institute for High Energy Physics, Serpukhov, SU-142284, Protvino, USSR

12 Institut für Hochenergiephysik, A-1050 Wien, Austria *)

*) Supported in part by Fonds zur Förderung der wissenschaftlichen Forschung.

## 1) Introduction

The lack of a consistent theory for soft hadronic physics is the reason why many models have been developed, each claiming to be able to describe correctly certain properties of the data in this field of particle physics. Current models use a quark-parton picture to explain the intrinsic mechanism of particle production, the most attractive ones being the LUND models [1] which have proven to be very successful in $e^+e^-$ physics and the Dual Parton models (DPM) [2,3] which are primarily designed to give insight into the mechanisms of low $p_T$ physics. The simple one chain LUND model and the simple two chain DPM have been extensively tested with hadron data. Such tests performed in terms of single particle distributions have been successful in many but not all cases [4,5]. Still there are open questions, for instance the failure to reproduce correctly charged multiplicity distributions and the seagull effect [6,7]. This has led to the development of more sophisticated models such as FRITIOF [8] and the Multichain DPM (MCDPM) [9]. It has been claimed that these come closer to a complete reproduction of the data. Models of more general phenomenological character have also been used to describe soft hadronic data, as for example, the cluster models which do not refer at all to the quark-parton structure of hadrons, but rather attempt to describe particle phenomena, without giving details of intrinsic particle production. The UA5 cluster model GENCL has proven to be very successful in describing single and double particle distributions of collider data [10].

The aim of this paper is to test these fragmentation models against experimental two particle distributions at medium energy in order to provide further discrimination between models. We start with a comparison of two particle correlation data to the one string LUND model and the two chain DPM. Such investigations have not yet been performed in low $p_T$ physics and the intention is to show the effect of going from one to two chain models. Since it has been assumed [11,12] that the main difference between $e^+e^-$ and soft hadron interactions (in the ISR energy range) may be due to the presence of two chains in hadron interactions as opposed to one chain in $e^+e^-$. We shall show in this paper that the simple models do not give a satisfactory interpretation. Therefore, we investigate further improvements by introducing QCD effects like gluon radiation and semihard scattering and/or by an extension to many chains. A comparison with the UA5 cluster model is also made.

In section 2 we give a description of the experimental apparatus and the data sample. Section 3 presents briefly the models, parameters and functions to describe correlations between two particles. A comparison of our experimental results with the model predictions is given in section 4. A discussion of our results and a comparison with similar results for $e^+e^-$ and $\mu p$ data is the subject of section 5. A summary and conclusions are presented in section 6.

## 2) Experimental Apparatus and Data Sample

The NA23 experiment was performed at the CERN SPS using the European Hybrid Spectrometer (EHS). This experiment used a proton beam of 360 GeV/c momentum (i.e. $\sqrt{s}$ = 26 GeV).

### 2.1) Brief description of the experimental apparatus

EHS consisted of the hydrogen filled Rapid Cycling Bubble Chamber (RCBC) placed in a magnetic field of 3.0T, together with a downstream spectrometer. The latter contained a six-plane proportional wire chamber, three drift chambers ($4x2m^2$), a magnetic field of 1.5T and three additional drift chambers ($2x1.3m^2$) used for track reconstruction. Furthermore, two devices for particle identification (SAD and ISIS) and two gamma detectors (IGD and FGD) were present. A trigger was used to select bubble chamber pictures which contain beam interactions. More details have been published elsewhere [13].

In our analysis we used mainly data from RCBC to reconstruct tracks with low and intermediate momentum and $V^0$'s. For fast tracks the forward drift chamber information was also used. To identify particles we used the large pictorial drift chamber ISIS.

The necessary corrections of the $V^0$ data and the particle identification with ISIS are outlined in the following subsections. The bias introduced by the trigger is significant only for low multiplicity events ($n_{ch}<8$). In order to exclude the bulk of such events from our analysis we selected charged multiplicities larger than six.

### 2.2) Identification of $K_S^0$ and $\Lambda$

$K_S^0$ and $\Lambda$ were identified by their decays in the bubble chamber

$$K_S^0 \rightarrow \pi^+\pi^-$$

$$\Lambda \rightarrow p\pi^- \ .$$

The treatment of $V^0$'s has been described in previous publications [14-18]. Corrections for decays outside the bubble chamber fiducial volume were made using the standard potential weight procedure. An investigation of the decay length distribution shows a loss for decay lengths close to zero. We have taken this into account in the weighting procedure. In order to avoid unreasonably large weights it is necessary to exclude regions where the $V^0$ detection efficiency is very small. For reactions with strange particle pairs we have restricted the sample to $p_{lab}$ ($K_S^0$) < 25 GeV/c and $p_{lab}$ ($\Lambda$) < 15 GeV/c. The same kinematic restrictions have been applied for the model predictions. For reactions with a $\Lambda$ accompanied by charged hadrons we have used only backward $\Lambda$.

## 2.3) Charged particle identification

The details of the procedure used are given in [19]. Its principal features are discussed briefly.

Two main problems arise:

1) When ISIS information is available, the probabilities for various mass hypotheses can be calculated, and from this information a statistical estimation of the production probability of various types of particles in various kinematic regions must be extracted.
2) For some particles no ISIS information is available. This is mainly related to ISIS acceptance and the results must be corrected accordingly.

The quantity $\ln I/I_o$, where I is the ionization for a particle of given momentum and mass and $I_o$ is the minimum ionization value, is approximately normally distributed [20]. In this experiment the standard deviation of the quantity $\ln I/I_o$ is approximated by $0.60/\sqrt{N}$ where N is the number of ionization samplings in ISIS. Ionization calibration curves as function of the laboratory momentum for various masses are given in [19,20].

Using the above information a $\chi^2$ is calculated for electron, $\pi$, K, proton mass hypotheses and converted into an "ISIS probability" (one degree of freedom).

As suggested in [21], the following criteria are applied to these ISIS probabilities:

1) all mass hypotheses with probability less than 1% were rejected,
2) all mass hypotheses with probability less than 1/2 of the best probability for the same track are also rejected.

A "unique" ISIS identification is achieved if one and only one mass hypothesis satisfies the above criteria.

The purity of our $\pi$, K, p "unique samples" was determined by using a Monte Carlo program incorporating the ISIS calibration curves and the experimental distribution of N as a function of laboratory momentum fig. 1a. Using this information, along with the corresponding information concerning "unique" $\pi$'s, it is possible to set up and solve a system of linear equations from which the true numbers of K's etc. can be calculated [21]. All this particle identification treatment is applied for particles with momentum between 5 and 50 Gev/c (dashed lines in fig. 1a).

The ratio of the numbers of tracks having ISIS information to the total number of tracks found in the bubble chamber as a function of laboratory momentum is found to be constant above 7 GeV/c (~60%) fig. 1b.

Below 7 GeV/c, ISIS acceptance deteriorates: this is taken into account by a correction factor between 5 and 7 GeV/c.

## 2.4) The experimental data sample

From an exposure of RCBC (160 000 pictures) we selected a data sample consisting of 10672 events containing at least one V° ($\Lambda$, $\overline{\Lambda}$, $K_S^0$, $\gamma$). The requirement that a V° (60% of them being $\gamma$) is associated with the event does not lead to any significant bias for the results presented below.

In the following, we consider reactions containing identified hadron pairs with opposite strangeness and/or opposite baryon numbers

| | | |
|---|---|---|
| $pp \rightarrow$ | $K_S^0 \Lambda + X$ | (1) |
| | $K_S^0\ K_S^0 + X$ | (2) |
| | $K_S^0\ K^{\pm} + X$ | (3) |
| | $\bar{p}p + X$ | (4) |
| | $\overline{\Lambda}\Lambda + X$ | (5) |

and reactions containing unidentified hadrons

| | | |
|---|---|---|
| $pp \rightarrow$ | $\Lambda h^{\pm} + X$ | (6) |
| | $h^+h^- + X$ | (7) |
| | $h^+h^+ + X$ | (8) |
| | $h^-h^- + X$ | (9) |

In these reactions, the $K_S^0$ and $\Lambda$ are identified among the $V^0$'s observed in the bubble chamber. The charged particles ($K^\pm$, $\bar{p}$, p) are identified using ISIS, as described above and the unidentified hadrons are labelled $h^+$, $h^-$ *). The EHS detector enables an unambiguous charge determination of >95% of these secondary particles.

A charged multiplicity dependent renormalization is introduced to correct for losses of events and/or for biases due to selection criteria. Each event is weighted in order to reproduce the topological cross sections of [13].

## 3) Description of Models and Two Particle Correlation Variables

At fixed energy the two particle cross section is a function of the following five independent variables: $y_1$, $y_2$, $|p_{T_1}|$, $|p_{T_2}|$ and $\phi$ where y is the rapidity and $\phi$ is the angle between the two transverse momentum vectors $\vec{p}_{T_1}$, $\vec{p}_{T_2}$ of a hadron pair $h_1$, $h_2$ (the incident beam particle is taken as the reference for the longitudinal direction).

### 3.1) Ordinary String Models and definition of the quantities

We will first compare the data with the original one string LUND model (called LUND in the following) and with a two string Dual Parton Model (called DPM). Both do not include diffractive dissociation.

Both models are available in the form of Monte-Carlo programs [22,23]. The DPM program uses the LUND fragmentation scheme for each chain separately **), thus there is no difference in the fragmentation mechanisms contained in both programs.

The relevant assumptions of these models are the following: quark-antiquark pairs are created in the color field of quark (diquark) jets with opposite transverse momentum $p_T$ with respect to the jet axis. The quark (antiquark) ends up in two hadrons $h_1$, $h_2$ of successive rank (fig. 2). Such hadrons are therefore predicted to be correlated

*) Lorentz transformations for $h^+$ and $h^-$ are made, assuming a pion mass for them.

**) Version 1.6 of the LUND Monte Carlo program has been used.

both in the direction of their transverse momenta and in rapidity.
To investigate the angular correlations we define the angle $\Phi$ in the following way:

$$\cos \Phi = \frac{\vec{k}_1 \cdot \vec{k}_2}{|\vec{k}_1| \cdot |\vec{k}_2|} \qquad (10)$$

$\vec{k}_1$, $\vec{k}_2$ being the momentum vectors of the hadrons $h_1$, $h_2$ in the transverse plane which is approximately perpendicular to the jet axis in our case. We shall use the asymmetry of the distribution $W(\Phi)$:

$$B = \frac{\int_{\frac{\pi}{2}}^{\pi} W(\Phi)d\Phi - \int_{0}^{\frac{\pi}{2}} W(\Phi)d\Phi}{\int_{0}^{\pi} W(\Phi)d\Phi} \qquad (11)$$

The overall conservation of transverse momenta in the final state leads to a value of B which is small, although nonzero, i.e. B=0.06 *) independently of hadron flavors and their rapidity gap $\Delta y = |y_{h_1} - y_{h_2}|$. According to the string fragmentation mechanism one expects a distribution $W(\Phi)$ showing a significant maximum at $\Phi = \pi$ [24]. It results from the assumption of local $p_T$ compensation at the quark level.
An analytical calculation [25] of $W(\Phi)$ for hadron pairs of successive rank yields B=0.5 **). The inclusion of hadron pairs with non-successive ranks and resonance production will reduce this value.
The LUND model and DPM include low mass resonances and uncorrelated background pairs in the simulation. They predict, as one may expect, that the transverse momentum correlation is largest for hadrons with a small rapidity gap ($\Delta y < 2$).
To investigate rapidity correlations for particle pairs with low statistics (e.g. $K_S^0$, $\Lambda$, $\bar{\Lambda}$) we use the correlation parameter $\rho$ [26]:

$$\rho_y = \frac{\mathrm{cov}\,(y_1, y_2)}{\sqrt{\mathrm{var}(y_1)\ \mathrm{var}(y_2)}} \qquad (12)$$

*) For a fixed multiplicity the formula for the B value expected from conservation of transverse momentum is given in [27]. The value 0.06 was obtained by using this relation and averaging over the charged multiplicity distribution, taking the average number of associated $\pi^0$ into account.

**) We obtained this result by taking $\sigma_q/\sigma_{qq} = 1$, assuming no diquark splitting and using eqn.(5) of [24] which was derived analytically for describing $p\bar{p}$ pair production. With these assumptions the same formula also applies here.

This is a measure of the linear dependence of the rapidities $y_1$ and $y_2$. The two extreme values of $\rho$ are: $\rho = 0$ if there is no correlation and $\rho = \pm 1$, if there is exact linear dependence between $y_1$ and $y_2$.
In contrast to $\rho$ which is a number, the correlation ratio $R(y_1, y_2)$, which we will use for particle pairs where high statistics are available (e.g. $h^+$, $h^-$), is a function containing the two particle distributions $d^2N/dy_1dy_2$ and the single particle distributions $dN/dy_{1,2}$. It is defined by the following equation [27]:

$$R(y_1,y_2) = \left(\frac{1}{N}\frac{d^2N}{dy_1dy_2}\right) / \left(\frac{1}{N}\frac{dN}{dy_1} \cdot \frac{1}{N}\frac{dN}{dy_2}\right) - 1 \qquad (13)$$

### 3.2) FRITIOF, MCDPM and the GENCL models

The FRITIOF model (version 3.1) contains two strings without color exchange between them. Therefore this model is designed to reproduce also diffractive events. Furthermore multigluon radiation and semihard scattering effects are included [8].
MCDPM produces in addition to the two chains between quark and diquarks of the incident particles several short chains out of the sea. The fragmentation is again performed according to the LUND fragmentation scheme. Here the production of diffractive events is excluded [9].
The UA5 cluster model GENCL is a new application of cluster models [28]. It does not give details about the intrinsic mechanisms of particle production. Clusters are produced according to phase space with a damping in transverse direction of exp $(-6p_T)$. Many features of the experimental $p\bar{p}$ data at $\sqrt{s}$ = 540 GeV are input to the model (e.g. rapidity-, multiplicity distribution). By using GENCL diffractive events are not considered [10].
All these models are used in form of Monte Carlo programs. For the MCDPM the still preliminary version 1.3 is used to show the trend of the development [29].

## 4) Experimental Data and Comparison with Models

In Table 1 we present experimental $\rho$ and B values for reactions with identified particles, i.e. $pp \to K_S^0\Lambda$, $K_S^0K_S^0$, $K_S^0K^\pm$, $\bar{p}p$, $\bar{\Lambda}\Lambda$ and for $pp \to \Lambda\pi^\pm$,

$\pi^+\pi^-$, $\pi^\pm\pi^\pm$. However, when interpreting these values one has to be aware that the cuts described in section 2 may introduce large changes especially in $\rho_y$. To compare the results meaningfully with model predictions we apply, in the following, the same cuts to the data and the models.

### 4.1) Correlations of hadron pairs with opposite strangeness and/or baryon numbers

The advantage of selecting pairs of particles with opposite strangeness and/or baryon numbers is that they contain mainly pairs with successive rank, since the probability at this energy for producing more than one pair of strange particles or baryons is very low. In order to test the assumption of local $p_T$ conservation intrinsic to the fragmentation mechanism of the string models such a sample of particle pairs is particularly useful.
In fig. 3 *) the parameters B (11) [30] and $\rho_y$ (12) are shown for reactions (1) to (5). Both models, the LUND and the DPM, tend to overestimate B and underestimate $\rho$.

### 4.2) Correlations for reactions with unidentified hadrons ($\Lambda h^\pm$, $h^+h^-$, $h^\pm h^\pm$)

#### 4.2.1) Azimuthal correlations

In the case of reactions (6) to (9) the background coming from the contamination of pairs with nonsuccessive rank is much higher, but still a significant correlation originating from hadron pairs of successive rank is predicted by the models in certain cases. In the following we present a comparison of data and models in terms of B versus $\Delta y$. The sample $\Lambda h^+$, $\Lambda h^-$ is shown in figs. 4a and 4b. Here the $\Lambda$ have been restricted to the target proton fragmentation region $x_\Lambda < -0.2$. A significantly different behavior of the data for $\Lambda h^+$ and $\Lambda h^-$ is observed. An increase of B at small $\Delta y$ is seen for $\Lambda h^+$ but not for $\Lambda h^-$. This difference can be attributed to the $\Lambda K^+$ pairs in the $\Lambda h^+$ sample which causes an increase of B at small $\Delta y$. In the

*) All Monte Carlo calculations have been performed with increased statistics (50.000 - 100.000 events) in order to reduce the error bar considerably in comparison to the data.

proton fragmentation region $\Lambda$'s are supposed [31] to be produced predominantly from the ud diquark of the proton and an s-quark from the sea. In this case they are frequently produced in association with a $K^+$ containing an $\bar{s}$-quark. Therefore such $\Lambda K^+$ pairs have successive rank. $\Lambda h^-$ pairs cannot contain a common $s\bar{s}$ quark pair. This sample represents therefore the behavior of nearly uncorrelated pairs *). The LUND model and DPM in fig. 4 both show qualitatively the same behavior. Whereas DPM reproduces the data rather well, LUND overestimates slightly the behavior of $\Lambda h^+$.

This interpretation receives further support from the results given in table 2. In this table B is given separately for $\Lambda$ produced in the fragmentation and in the central region. One observes a smaller or even no increase of B at small $\Delta y$ in the central region for $\Lambda h^+$. Both models predict this difference between the fragmentation and central region. The relevant assumption is that centrally produced $\Lambda$ frequently contain a diquark from the sea and are created in association with an antibaryon (antihyperon or antiproton). We note that LUND predictions lie systematically above the experimental data. The sample $h^+h^-$ includes pairs with common $u\bar{u}$ or $d\bar{d}$. However, in this case the background from uncorrelated pairs is larger than for the $\Lambda h^+$ sample. B versus $\Delta y$ is shown in fig. 5 for $h^+h^-$ (5a, 5b), $h^+h^+$ (5c) and $h^-h^-$ (5d) pairs. Fig. 5a contains all charged multiplicities $n_{ch}$ whereas fig. 5b is restricted to $n_{ch} \geq 6$ to suppress diffractive events and to $n_{ch} \leq 12$ to reduce the combinatorial background generated at high multiplicities. Going from fig. 5a to 5b one observes a more significant increase of B, at least for the experimental data at small $\Delta y$. Both models overestimate the rise at small $\Delta y$. The DPM predictions go, however, in the right direction. Since both models fail to reproduce the overall multiplicity distribution **) one could suspect that the observed discrepancy in B is at least partially due to multiplicity effects. In order to investigate the influence of this particular defect of the models the observed

*) In both cases the influence of $\Sigma^*(1385)$ has been removed by excluding $\Lambda h^\pm$ pairs with $1.36 \leq m(\Lambda h^\pm) < 1.41$ GeV.

**) A comparison with the experimental multiplicity distribution ($\langle n_{ch} \rangle = 9.06 \pm 0.09$, dispersion $D = 4.49 \pm 0.05$ [11]) shows that the multiplicity distribution of the LUND Monte Carlo is much too narrow ($\langle n_{ch} \rangle = 7.4 \pm 0.01$, $D = 2.47 \pm 0.03$) whereas the one of the DPM Monte Carlo is much better but still not good enough ($\langle n_{ch} \rangle = 8.76 \pm 0.01$, $D = 3.65 \pm 0.06$) [32].

multiplicity distribution for $6 \leq n_{ch} \leq 12$ has been imposed to the models by weighting the semi-inclusive channels appropriately . The curves in fig. 5b show that both models still overestimate B at small $\Delta y$.

For $h^+h^+$ and $h^-h^-$ pairs no rise at small $\Delta y$ is observed experimentally. The Bose-Einstein correlation causes a decrease of B for $\Delta y < 1$. This effect is not included in the models. However, we obtain a rough estimate of its influence in the following way: We introduce the Bose-Einstein effect into the DPM Monte Carlo program by weighting events containing $h^+h^+$ or $h^-h^-$ pairs with small momentum differences with a weight factor > 1. The weights have been chosen to reproduce the well known effect in the $q_T$ and $q_L$ distributions [33]. The resulting decrease of $B(h^\pm h^\pm)$ for $\Delta y < 2$ is about 20%, in approximate agreement with the data in figs. 5c, 5d. We conclude therefore that if DPM included this effect it would reproduce reasonably well the B values of the $h^-h^-$ pairs. In the case of $h^+h^+$ pairs both models overestimate B at small $\Delta y$. The difference between $h^+h^+$ and $h^-h^-$ pairs predicted by the models is not seen in the data.

For these particle pairs the behaviour of B as a function of $p_T$ has also been investigated. Fig. 6 shows the data compared to LUND and DPM predictions as a function of $|p_{T_1}| + |p_{T_2}|$, the sum of the absolute values of the transverse momenta of the two particles considered. Although the data for like sign (fig. 6b) and unlike sign (fig. 6a) pairs are in good agreement with each other, the LUND predictions diverge significantly from them for increasing $|p_{T_1}| + |p_{T_2}|$. Only the DPM predictions for like sign pairs are in agreement with the data (fig. 6b).

#### 4.2.2) Rapidity correlations

Two particle pseudorapidity correlation data in the ISR energy region have been investigated extensively in the past [34]. Two particle rapidity correlation data from the ISR at $\sqrt{s}$=53 GeV have been published more recently [35]. Such data show a tremendous power of discrimination between models as will be demonstrated in this subsection. We present our data and also the model predictions in terms of the correlation ratio R (13).

We restrict this part of the analyses to reactions with good statistics, i.e. (7), (8), (9). We consider particles in the following combinations: charged-charged (cc), plus-plus (++), minus-minus (--)

and plus-minus (+-). We consider only charged multiplicities $n_{ch} > 6$. A comparison of $R^{cc}(y_1, y_2 = \pm 1,0)$ and $R^{++,--,+-}(y_1, y_2 = 0)$ to ISR data at $\sqrt{s}$=53 GeV [35] shows agreement within error bars. The energy independence of R(0,0) was already noticed over the ISR energy region. The energy dependence of the maximum rapidity $y_{max}$ demands that our data lie below the ISR data ($\sqrt{s}$=53 GeV) if $y_1, y_2 \neq 0$.

Figs. 7a shows $R^{cc,--,++,+-}(y_1, y_2 = 0)$ versus $y_1$. One observes a large disagreement of the models with the data. For $h^-h^-$ and $h^+h^+$ pairs the models even predict negative correlations very much in contrast to the data. An estimate of the contribution of the Bose-Einstein effect using the method mentioned above would move the model predictions to more positive values by at most 20% on the average and can therefore not explain the observed large discrepancies.

$R^{cc}(y_1, y_2 = \pm 1.5, \pm 1)$ versus $y_1$ is shown in fig. 7b. Again strong disagreement with LUND and DPM predictions are observed.

A comparison of multiplicity corrected DPM *) with our data in terms of $R(y_1, y_2 = 0)$ is shown in fig. 8. Such a correction reduces significantly the discrepancy between the model predictions and the data, but is not enough to explain the failure of the models to reproduce the experimental data.

### 4.3) Comparison with FRITIOF, MCDPM and GENCL

In the previous considerations we have observed that there are large discrepancies between the predictions of the ordinary string models and the experimental data. This is true both for azimuthal and for rapidity correlations. Furthermore, we have shown that these discrepancies are in part due to the limited ability of the ordinary string models to reproduce the charged multiplicity distribution of the data.

Fig. 9 shows topological cross sections versus the charged multiplicity $n_{ch}$ for MCDPM 1.3 **), GENCL, FRITIOF 3.1 and our data. A comparison of these distributions is only possible by taking into account the

*) The weigthing method mentioned in 4.2.1) has been applied.
**) The number of chains is limited to $\leq 10$.

fact that MCDPM and GENCL do not include diffractive events, whereas FRITIOF and NA23 data do. The program GENCL contains a negative binomial distribution which is in agreement with the nondiffractive part of the NA23 data. FRITIOF for $n_{ch} \geq 8$ is in much better agreement with the data than LUND. Only MCDPM produces too many high multiplicity events *) ($\langle n_{ch} \rangle$ = 11.52±0.01, D=4.1±0.08).

The correlation properties of these models are shown in fig. 10. Here we consider the parameter B (11) and the function R (13) for the reactions (7) to (9) which have high statistics.

B versus $\Delta y$ is shown in fig. 10a for reaction (7). GENCL, FRITIOF and MCDPM give a much better agreement with the data than LUND and DPM.

Fig. 10b shows $R(y_1,y_2=0)_{CC,--,++,+-}$ versus $y_1$. FRITIOF and MCDPM reproduce the data much better than the ordinary LUND model, but the cluster model GENCL gives an even better description of the data. The MCDPM provides only a moderately improved description of the data.

Similar observations apply also to the case of $R(y_1,y_2=\pm 1.5,\pm 1.)_{CC}$.

## 5) Discussion

We note that the ordinary models LUND and DPM do not describe correctly the observed correlations in azimuthal angle and in rapidity.

In contrast with our results, similar correlation measurements in $e^+e^-$ [12] and $\mu p$ [36] reactions have shown agreement with a LUND fragmentation model.

Concentrating first on the $e^+e^-$ case we find that there a LUND model has been used which contains a so-called "bare" string fragmentation of the $q\text{-}\bar{q}$ quark system (corresponding to our ordinary LUND model), but with QCD effects such as multiple soft gluon emission and hard gluon emission included. A comparison of our results on $R(y_1,y_2=0)_{CC}$ with $e^+e^-$ results is presented in fig. 11a. The $e^+e^-$ results are shown only near $y_1=0$. The striking feature seen in this figure is that if one were to use the LUND model with the "bare" $q\text{-}\bar{q}$ fragmentation (without the QCD effects) then also for $e^+e^-$ reactions one would observe a similar discrepancy between experimental data and this LUND model as we observe in fig. 7.

In the case of $\mu p$ data B for $\Delta y<1$ is presented in fig. 11b together with

*) By limiting the number of chains to ≤ 4 the number of high multiplicities is still overestimated ($\langle n_{ch} \rangle$ = 10.65±0.02, D = 3.5±0.08).

some of our results. The LUND model used in this case consisted of a bare string fragmentation of a q-qq system plus QCD effects and the introduction of a primordial transverse momentum ($\langle k_T \rangle$=0.44 GeV/c) [37]. If one had used in this case only the bare string fragmentation to calculate B for $\Delta y<1$, then one would have obtained a value very close to the one we have obtained in this work as demonstrated in fig. 11b.

From this we conclude that similar discrepancies as in this work would occur also for $e^+e^-$ and $\mu p$ reactions if QCD effects or primordial $k_T$ had not been taken into account. This suggests that such effects should be added to the LUND model of chapter 3.1 *). The FRITIOF model is a development in this direction and, as demonstrated in fig. 10, the improvement is promising **).

A further development of the ordinary DPM is proposed by the MCDPM [9]. In many cases the DPM reproduces our data better than the LUND model. This is particularly the case in the fragmentation region ($\Delta h^+$, $\Delta h^-$ (fig.4)). The multiplicity distribution of the DPM is closer to the experimental one, just by virtue of the presence of two chains. This suggests that more chains should be included already at our energies [9]. Fig. 10 shows also an improvement by a MCDPM compared to the DPM. Recently, it has been also shown that at an ISR energy of $\sqrt{s}$ = 62GeV rapidity correlations can be reasonably well described by such a multichain model [38].

In [39] a very good description of longitudinal and transverse correlation data at ISR energies was obtained using a model in which charged clusters are produced with limited charge exchange and a mean transverse momentum of 0.65 GeV/c. A comparison of our data with GENCL is also shown in fig. 10. The agreement with the data is striking.

## 6) Summary and Conclusion

In our data sample we find short range two particle correlations in the transverse plane and in rapidity. They are in agreement with the limited amount of information which was available before this experiment ($h^+h^-$, $h^\pm h^\pm$ pair correlations) and show flavour dependence which is expected from the string fragmentation scheme ($\Delta h^+$ and $\Delta h^-$ pairs). The comparison

*) Similar conclusions in terms of the seagull effect have been published recently [6].

**) It has been shown that FRITIOF correctly reproduces two particle correlation data at 900 GeV/c [40].

of our correlation data with the models in terms of B, $\rho$ and R provides insight into shortcomings and/or improvements of these models:

- the simple one string (LUND) and two string (DPM) models in general overestimate correlations in the transverse plane and underestimate them severely in rapidity;
- these discrepancies between the models and the data cannot only be attributed to the incorrect predictions for the multiplicity distributions;
- they can be reduced either by taking into account QCD effects in the fragmentation mechanism (FRITIOF), as also found for $e^+e^-$ and $\mu p$ reactions, or by introduction of more chains (MCDPM);
- the cluster model GENCL reproduces the correlation properties of our data well, without further tuning than the one provided by the authors to fit ISR and $S\bar{p}pS$ collider data.

In conclusion one can say that QCD effects such as multigluon radiation and the onset of hard scattering as well as the introduction of more strings constitute an improvement of the mentioned models in reproducing two particle correlation data and multiplicity distributions. But still the description of these data is not yet satisfactory, and other effects like cluster formation should be considered seriously also in quark parton models in low $p_T$ physics.

**Acknowledgement**

We would like to acknowledge the painstaking work of our scanning and measuring operators of the various laboratories of our collaboration, the technical teams involved with the bubble chamber, downstream spectrometer and SPS operations. We thank for many valuable discussions with B. Andersson, A. Capella, B. Holl and W. Kittel.

## References


1 B. Andersson, G. Gustafson, I. Holgersson, O. Månsson: Nucl. Phys. B178 (1981) 242.

2 G. Cohen-Tannoudji et al.: Phys. Rev. D19 (1979) 3397.

3 A. Capella, U. Sukhatme and J. Tran Thanh Van: Z. Phys. C3 (1980) 329;
T. Hirose: Proc. of the XXIInd Rencontre de Moriond on Hadrons, Quarks and Gluons, Les Arcs, Savoie/France, March 1987.

4 E. DeWolf: Proc. of the XIIIth International Symposium on Multiparticle Dynamics, Volendam/The Netherlands, 1982, p. 471;
E. DeWolf: Proc. of the XVth International Symposium on Multiparticle Dynamics, Lund/Sweden, 1984, p. 2.

5 W.G. Ma et al.: Z. Phys. C30 (1986) 191.

6 I.V. Ajinenko et al.: Phys. Lett. B197 (1987) 457.

7 J.L. Bailly et al.: Z. Phys. C35 (1987) 295;
W. Kittel: Proc. of the XVIth Symposium on Multiparticle Dynamics, Kiryat Anavim/Israel, 1985, p. 417;
W. Kittel: Proc. of the XXIst Rencontre de Moriond, Strong Interactions and Gauge Theories, Les Arcs - Savoie/France, 1986, p. 205;
P.A. van Hal: Proc. of the XVIIth International Symposium on Multiparticle Dynamics, Seewinkel/Austria, 1986, p. 533.

8 B. Andersson, G. Gustafson, B. Nilsson-Almqvist "A High Energy String Dynamics Model for Hadronic Interactions" FRITIOF 3.0: LU-TP 87-6;
B. Nilsson-Almqvist and Evert Stenlund, FRITIOF 1.6: LU-TP 86-14;
B. Andersson, G. Gustafson, B. Nilsson-Almqvist: Nucl. Phys. B281 (1987) 289.

9 A. Capella, J. Tran Thanh Van: Phys. Lett. 93B (1980) 146; Z. Phys. C10 (1981) 249.

10 G.J. Alner et al.: Nucl. Phys. B291 (1987) 445.

11 W. Koch: Proc. of the XIIIth International Symposium on Multiparticle Dynamics, Volendam/The Netherlands, 1982, p. 534.

12 TASSO Collaboration, M. Althoff et al.: Z. Phys. C29 (1985) 347.

13 J.L. Bailly et al.: Z. Phys. C23 (1984) 205.

14 M. Asai et al.: Z. Phys. C27 (1985) 11.

15 T. Aziz et al.: Z. Phys. C30 (1986) 381.

16 M. Asai et al.: Z. Phys. C34 (1987) 429.

17 S. Banerjee and A. Gurtu: Tata Inst. Report, TIFR-BC-83-7 (1983).

18 J. MacNaughton: Vienna int. report HEPHY-PUB 511/87.

19 J. MacNaughton and J.L. Bailly: Vienna int. report HEPHY-PUB 512/87.

20 W.W. Allison et al.: Nucl. Instr. & Meth. 224 (1984) 396.

21 S. Banerjee and J.B. Singh: CERN-EP 2742R (1985).

22 T. Sjöstrand: Comp. Phys. Comm. 39 (1986) 347.

23 A. Capella: private communication

24 A. Bartl, H. Fraas, H.R. Gerhold, W. Majerotto: Phys. Lett. 122B (1983) 427.

25 H.R. Gerhold: private communication

26 W.T. Eadie et al.: Statistical Methods in Experimental Physics, North Holland Publishing Company, Amsterdam (1971) p. 20.

27 J. Ranft and G. Ranft: Proc. of the Vth International Symposium on Many Particles Hadrondynamics, Eisenach/DDR (1974) p. 393.

28 E. Berger: Nucl. Phys. B85 (1975) 61.

29 A. Capella, J. Tran Thanh Van, T. Kreuzberger, P. Lipa: private communication

30 H. Dibon: Proc. of the XVIIth International Symposium on Multi-particle Dynamics, Seewinkel/Austria, 1986, p. 595.

31 J.L. Bailly et al.: Z. Phys. C31 (1986) 367.

32 H. Adamus et al.: Z. Phys. C.37 (1988) 215.

33 T. Åkesson et al.: Phys. Lett. 129B (1983) 269.

34 H. Dibon et al.: Phys. Lett. 44B (1973) 313;
G. Bellettini et al.: Phys. Lett. 45B (1973) 69;
L. Foa: Phys. Rep. 22C (1975) 1;
S.R. Amendolia et al.: Phys. Lett. 48B (1974) 359.

35 A. Breakstone et al.: Phys. Lett. 114B (1982) 383.

36 EMC Collaboration, M. Arneodo et al.: Z. Phys. C31 (1986) 333.

37 N. Schmitz, MPI, München: private communication

38 P. Aurenche, F.W. Bopp and J. Ranft: Z. Phys. C23 (1984) 67.

39 D. Drijard et al.: Nucl. Phys. B155 (1979) 269.

40 C. Fuglesang "Particle Production at the CERN $\bar{p}p$ Collider": Doctoral Dissertation 1987; Institute of Physics, University of Stockholm.

## Figure Captions

Fig. 1a: The probabilities calculated by a Monte Carlo program that $\pi$'s, K's and protons having ISIS information will be assigned to "unique" proton (upper plots) and "unique" K (lower plots) as a function of laboratory momentum. The region between the dashed lines is the region where ISIS information was used.

Fig. 1b: The ratios of the number of tracks having some ISIS information to the number of tracks found in the RCBC as a function of laboratory momentum for positive and negative tracks.

Fig. 2: Quark fragmentation lines for production of hadron pairs $h_1$, $h_2$ and strange-antistrange hadron pairs according to cascade models.

Fig. 3: Experimental data compared with LUND and DPM model predictions for B with $\Delta y < 2$ (fig. 3a) and $\rho_{y\_}$ (fig. 3b) for the particle combinations $\Lambda K_S^0$, $K_S^0 K_S^0$, $K_S^0 K^\pm$, $\bar{p}p$, $\bar{\Lambda}\Lambda$.

Fig. 4: Experimental values of B as a function of $\Delta y$ for reaction (6) compared with predictions of the LUND and DPM models ($x_\Lambda < -0.2$).

Fig. 5: B as a function of $\Delta y$ for reactions (7)-(9). For fig. 5b only, the LUND and DPM predictions have been modified by renormalizing to the experimental charged multiplicity distribution for $6 < n_{ch} < 12$.

Fig. 6: B versus $|p_{T_1}| + |p_{T_2}|$ for
a) unlike sign hadron pairs $h^+h^-$;
b) like sign hadron pairs $h^+h^+ + h^-h^-$.

Fig. 7: a) $R^{cc}$, $--$, $++$, $+-(y_1, y_2 = 0)$ NA23 experimental data compared to the predictions of the LUND and the DPM model for $n_{ch} > 6$;
b) $R(y_1, y_2 = -1.5, -1., 1., 1.5)$ NA23 experimental data for charged-charged (cc) combinations compared to the predictions of the LUND and the DPM model for $n_{ch} > 6$.

Fig. 8: $R^{cc}$, $--$, $++$, $+-(y_1, y_2 = 0)$ NA23 experimental data compared to the multiplicity corrected DPM predictions for $n_{ch} > 6$.

Fig. 9: Topological cross sections versus $n_{ch}$ for MCDPM 1.3, GENCL, FRITIOF 3.1 and NA23 data.

Fig. 10: Comparison of NA23 data with predictions of the MCDPM 3.1, the GENCL with average cluster size 1.8 and the FRITIOF 3.1..
a) B versus $\Delta y$ for $h^+h^-$;
b) $R^{cc,--,++,+-}(y_1, y_2 = 0)$ versus $y_1$.

Fig. 11: Comparison of NA23 data with results of $e^+e^-$ (TASSO), $\mu p$ (EMC) and their LUND model predictions.
a) $R(y_1, y_2=0)_{cc}$ compared with $R(y_1 \approx 0, y_2=0)_{cc}$ of the TASSO [12] collaboration. LUND and "bare" LUND $e^+e^-$ (without QCD effects).
b) B versus $\Delta y$ for $h^+h^-$:
- NA23 data compared with $\mu p$ data of the EMC [36],
- LUND compared to "bare" LUND (without QCD effects and primordial $k_T$).

Table 1: Experimental values for $\rho_y$, $\rho_{pT}$ and B of several particle pairs.

| | $\rho_y$ | $\rho_{pT}$ | B($\Delta y<2$) | No. of pairs |
|---|---|---|---|---|
| $K_S^oK_S^o$ | 0.28±0.08 | 0.05±0.11 | −0.05±0.12 | 75 |
| $\Lambda K_S^o$ | 0.08±0.12 | 0.04±0.12 | 0.03±0.14 | 100 |
| $\Lambda\bar{\Lambda}$ | 0.53±0.13 | 0.08±0.26 | −0.28±0.27 | 18 |
| $K_S^oK^+, K_S^oK^-$ | 0.20±0.09 | 0.06±0.11 | 0.20±0.12 | 74 |
| $\Lambda\pi^+$ | 0.04±0.05 | 0.10±0.05 | 0.07±0.07 | 374 |
| $\Lambda\pi^-$ | 0.02±0.05 | 0.07±0.06 | 0.16±0.07 | 345 |
| $\pi^+\pi^-$ | 0.07±0.02 | 0.03±0.01 | 0.08±0.02 | 3966 |
| $p\bar{p}$ | 0.10±0.2 | 0.43±0.10 | 0.35±0.16 | 29 |
| $\pi^+\pi^+$, $\pi^-\pi^-$ | 0.27±0.01 | 0.03±0.02 | 0.03±0.02 | 3154 |

**Table 2:** B values for $\Lambda h^+$, $\Lambda h^-$ for $|\Delta y| < 2$ and $\Sigma(1385)$ excluded.

$x_\Lambda < -0.2$ (fragmentation):

| | exp. | LUND | DPM |
|---|---|---|---|
| $\Lambda h^+$ | .19±.03 | .30±.01 | .19±.01 |
| $\Lambda h^-$ | .03±.04 | .06±.02 | .07±.02 |

$-0.2 < x_\Lambda < 0$ (central):

| | exp. | LUND | DPM |
|---|---|---|---|
| $\Lambda h^+$ | .09±.04 | .15±.02 | .12±.02 |
| $\Lambda h^-$ | .07±.05 | .17±.03 | .07±.02 |

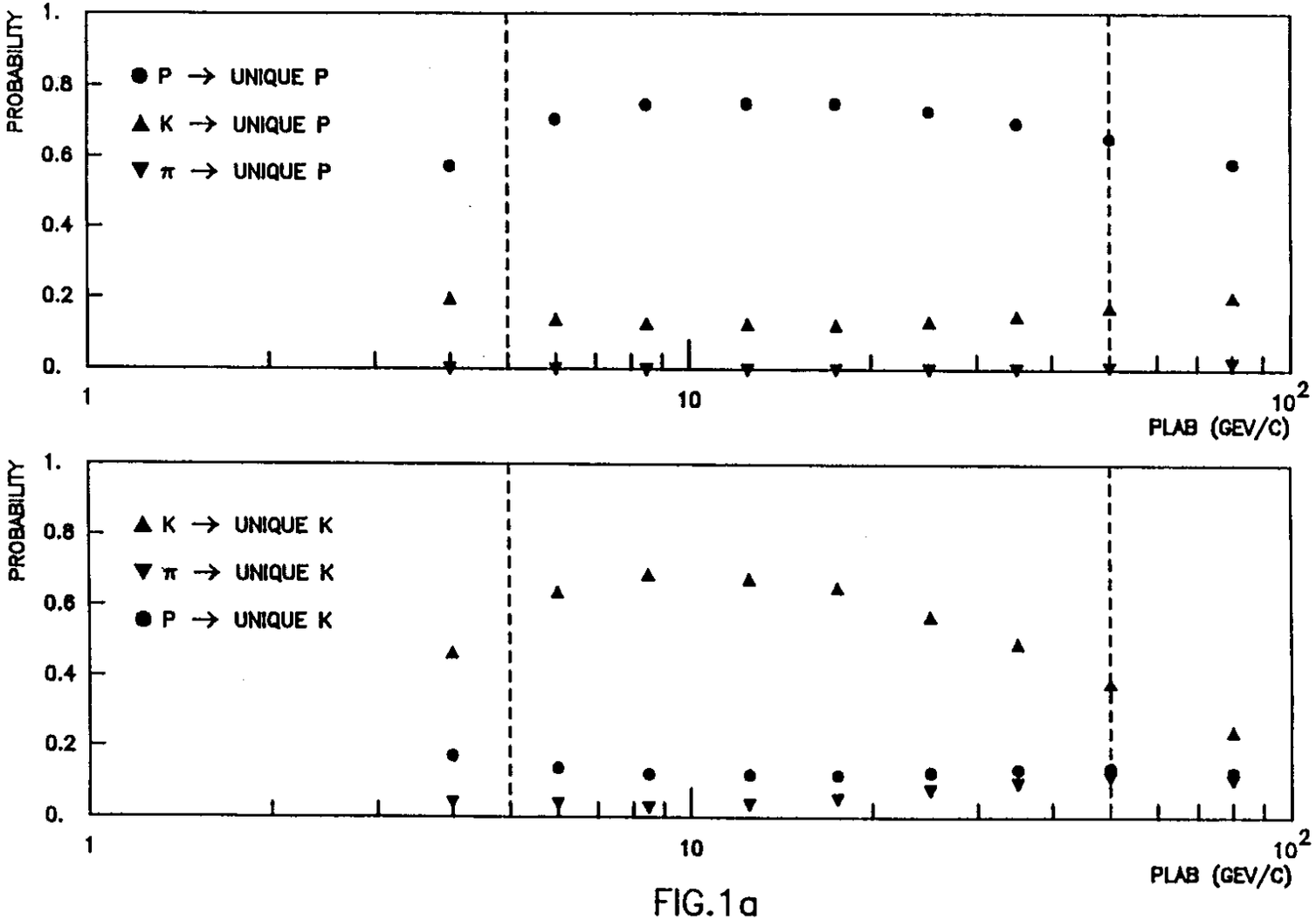
PROBABILITY
1.
0.8
0.6
0.4
0.2
0.
● P → UNIQUE P
▲ K → UNIQUE P
▼ π → UNIQUE P
1
10
10^2
PLAB (GEV/C)
PROBABILITY
1.
0.8
0.6
0.4
0.2
0.
▲ K → UNIQUE K
▼ π → UNIQUE K
● P → UNIQUE K
1
10
10^2
PLAB (GEV/C)

FIG.1a

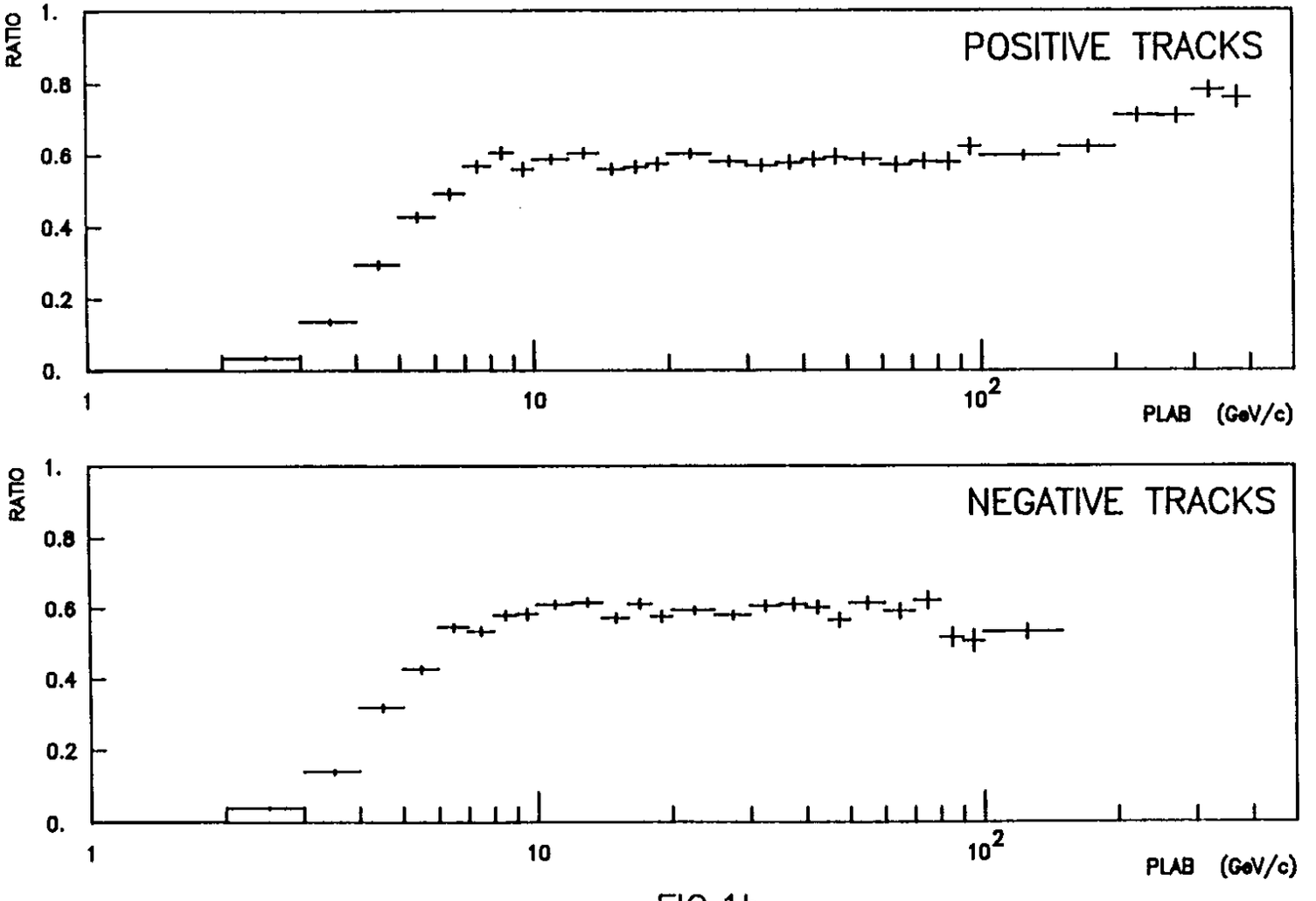
POSITIVE TRACKS
RATIO
1.
0.8
0.6
0.4
0.2
0.
1
10
$10^2$
PLAB (GeV/c)
NEGATIVE TRACKS
RATIO
1.
0.8
0.6
0.4
0.2
0.
1
10
$10^2$
PLAB (GeV/c)

FIG.1b

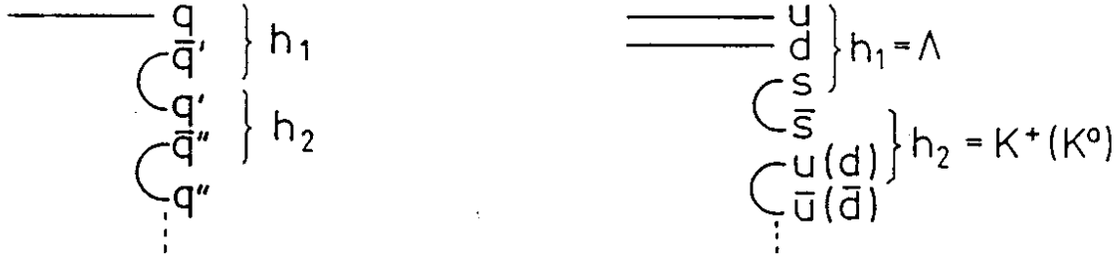


Fig.2

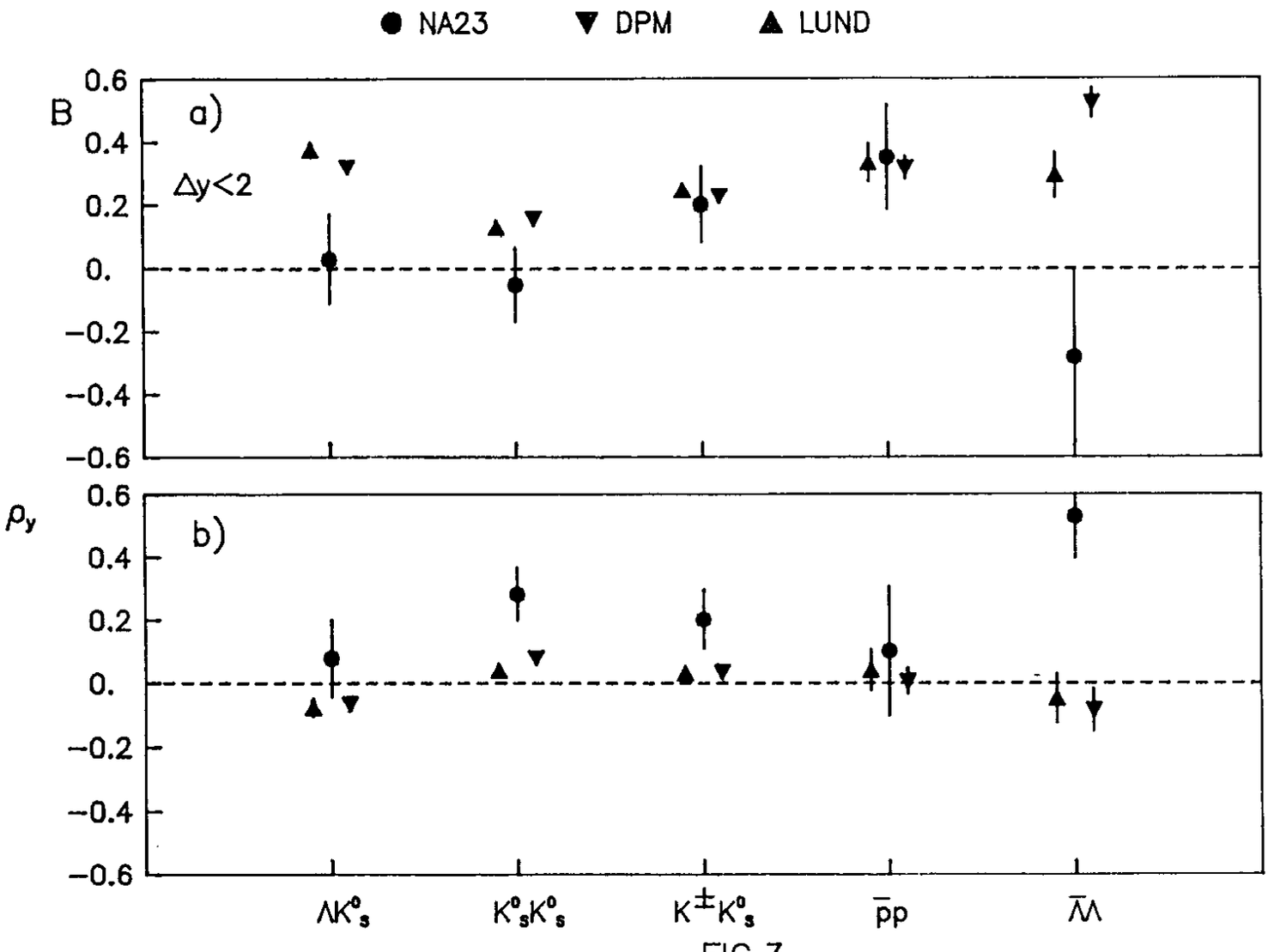
NA23
DPM
LUND
B
a)
Δy<2
0.6
0.4
0.2
0.
−0.2
−0.4
−0.6
$\rho_y$
b)
0.6
0.4
0.2
0.
−0.2
−0.4
−0.6
$\Lambda K^0_s$
$K^0_s K^0_s$
$K^{\pm} K^0_s$
$\bar{p}p$
$\bar{\Lambda}\Lambda$

FIG.3

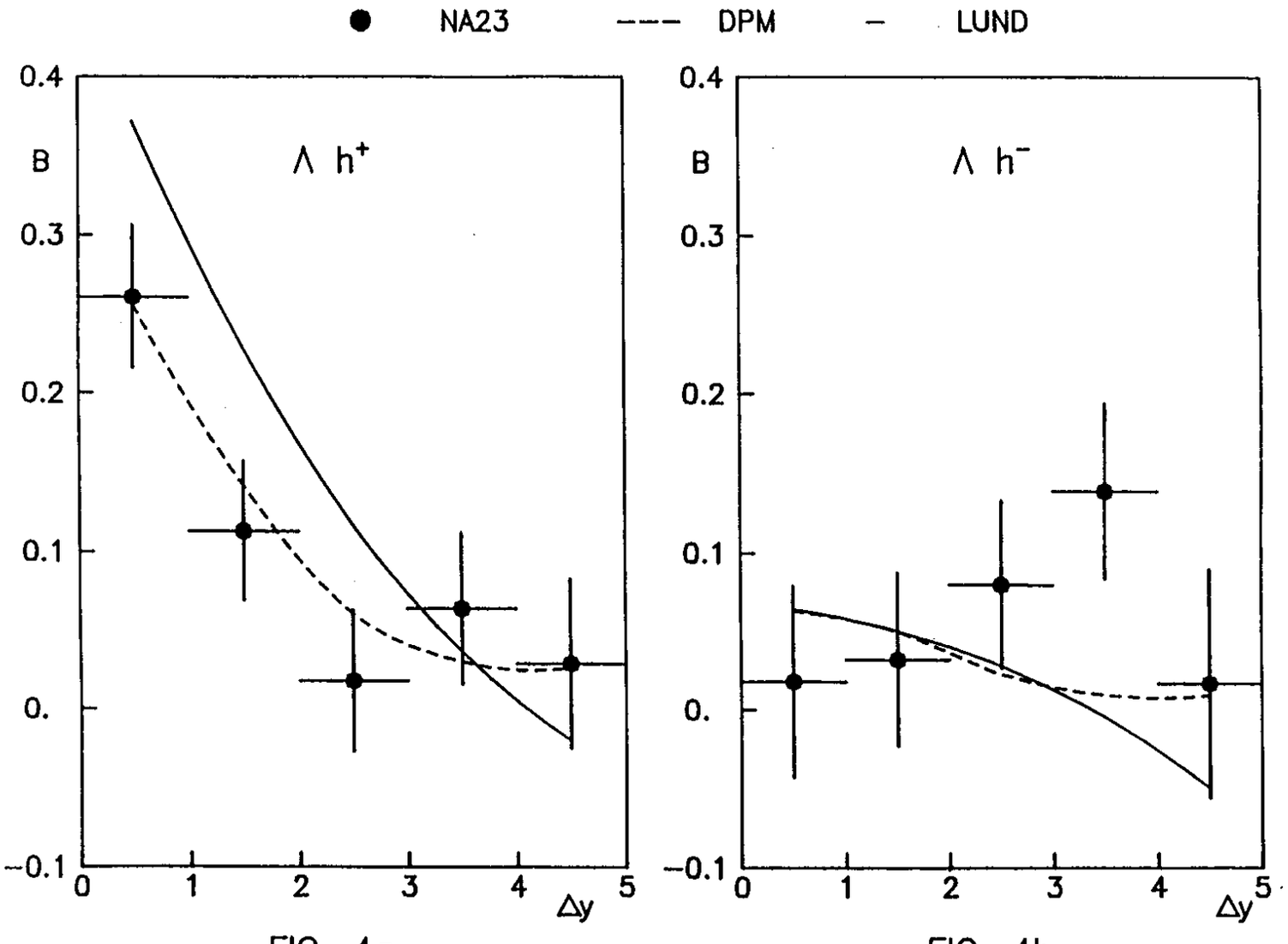


FIG. 4a

FIG. 4b

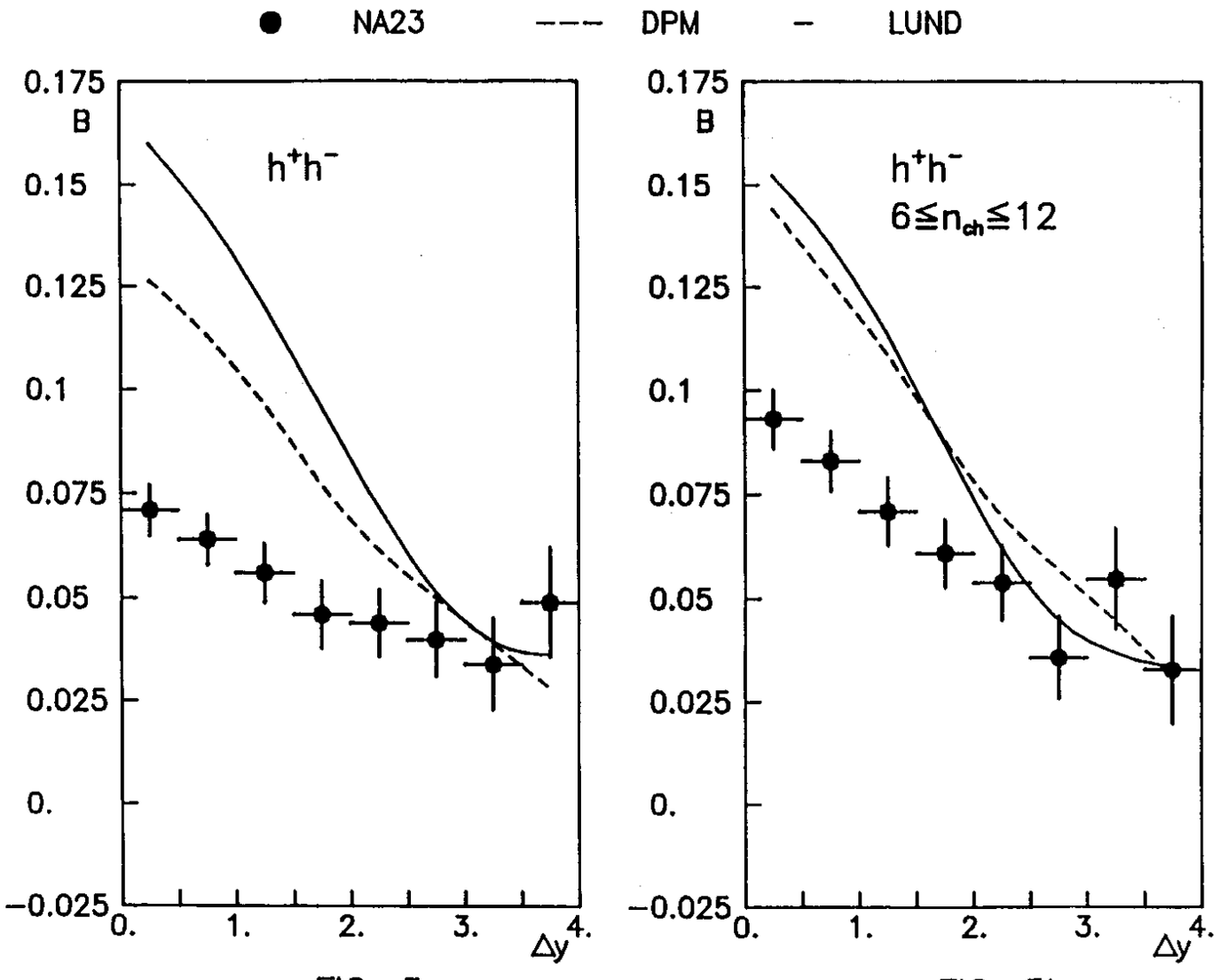
NA23
DPM
LUND
B
h⁺h⁻
0.175
0.15
0.125
0.1
0.075
0.05
0.025
0.
-0.025
0.
1.
2.
3.
4.
Δy

FIG. 5a


B
h⁺h⁻
6≦n_ch≦12
0.175
0.15
0.125
0.1
0.075
0.05
0.025
0.
-0.025
0.
1.
2.
3.
4.
Δy

FIG. 5b

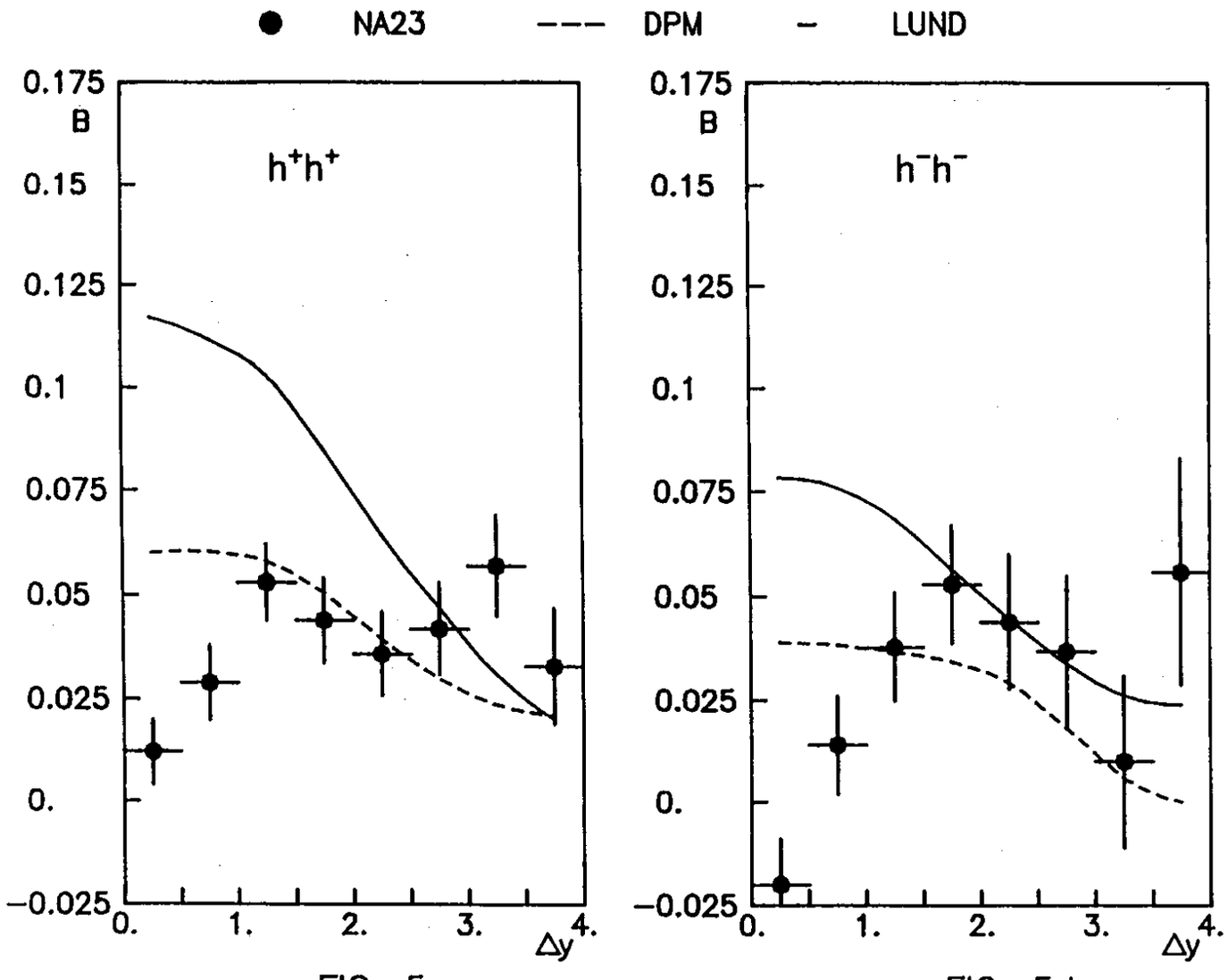
NA23
DPM
LUND
B
$h^+h^+$
$h^-h^-$
0.175
0.15
0.125
0.1
0.075
0.05
0.025
0.
−0.025
0.
1.
2.
3.
4.
Δy

FIG. 5c

FIG. 5d

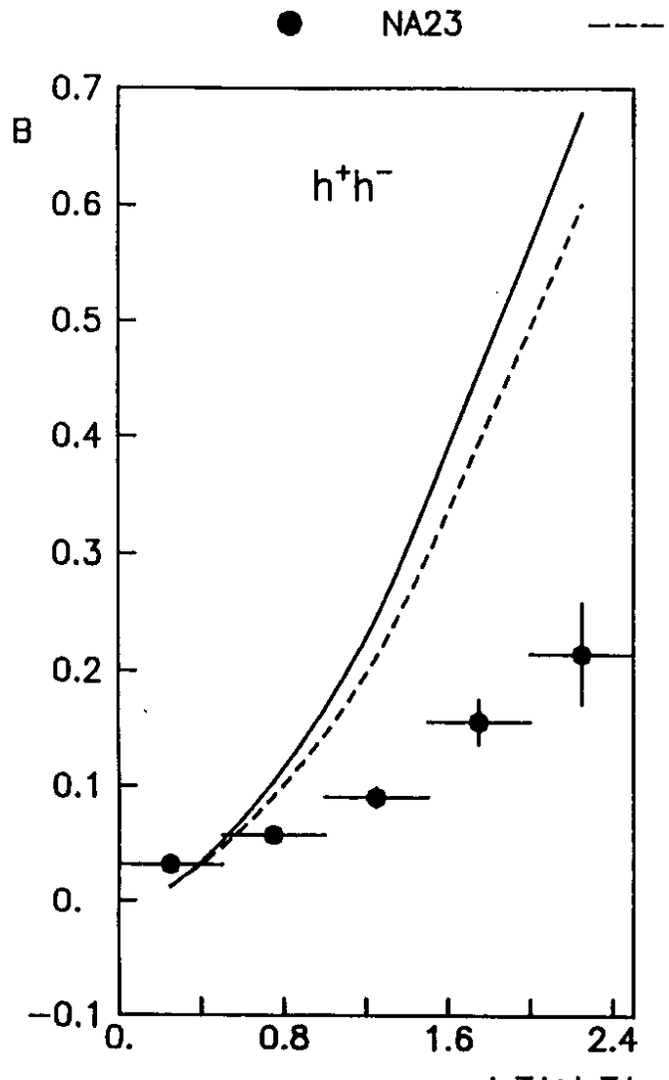
NA23
DPM
LUND
B
0.7
0.6
0.5
0.4
0.3
0.2
0.1
0.
−0.1
$h^+h^-$
0.
0.8
1.6
2.4
$|pT_1|+|pT_2|$

FIG. 6a

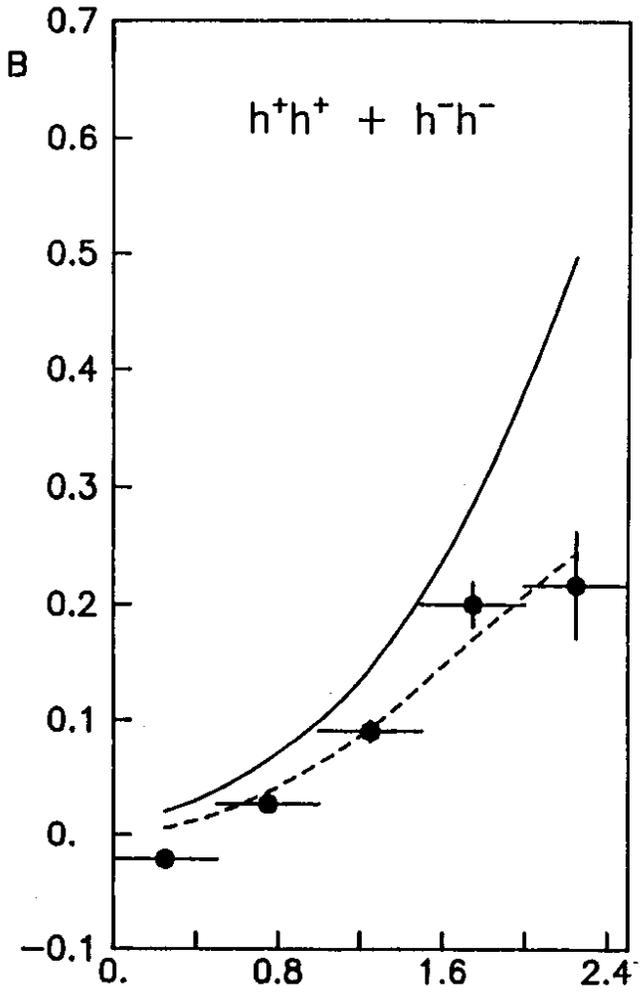
B
0.7
0.6
0.5
0.4
0.3
0.2
0.1
0.
−0.1
$h^+h^+ + h^-h^-$
0.
0.8
1.6
2.4
$|pT_1|+|pT_2|$

FIG. 6b

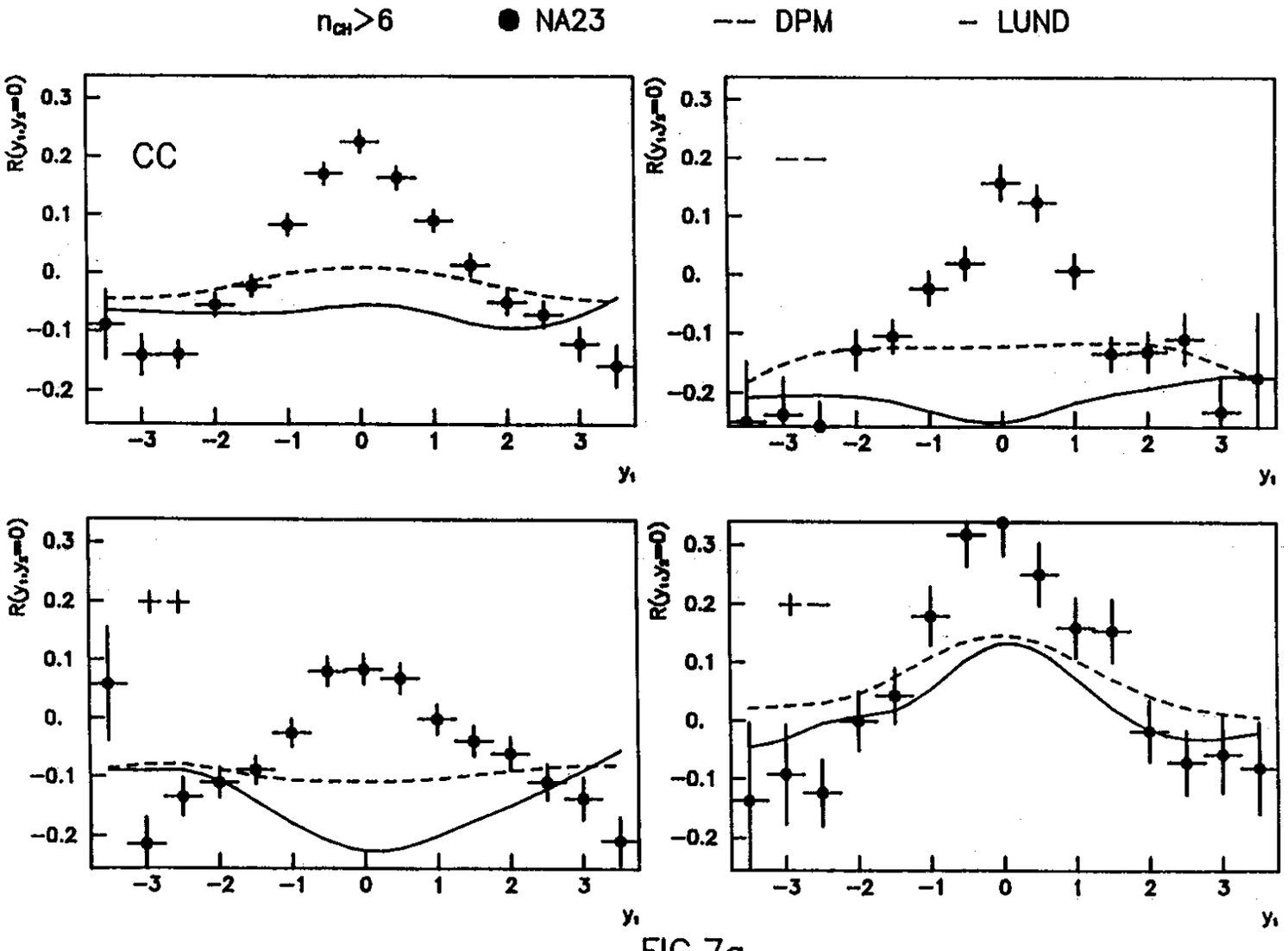


FIG.7a

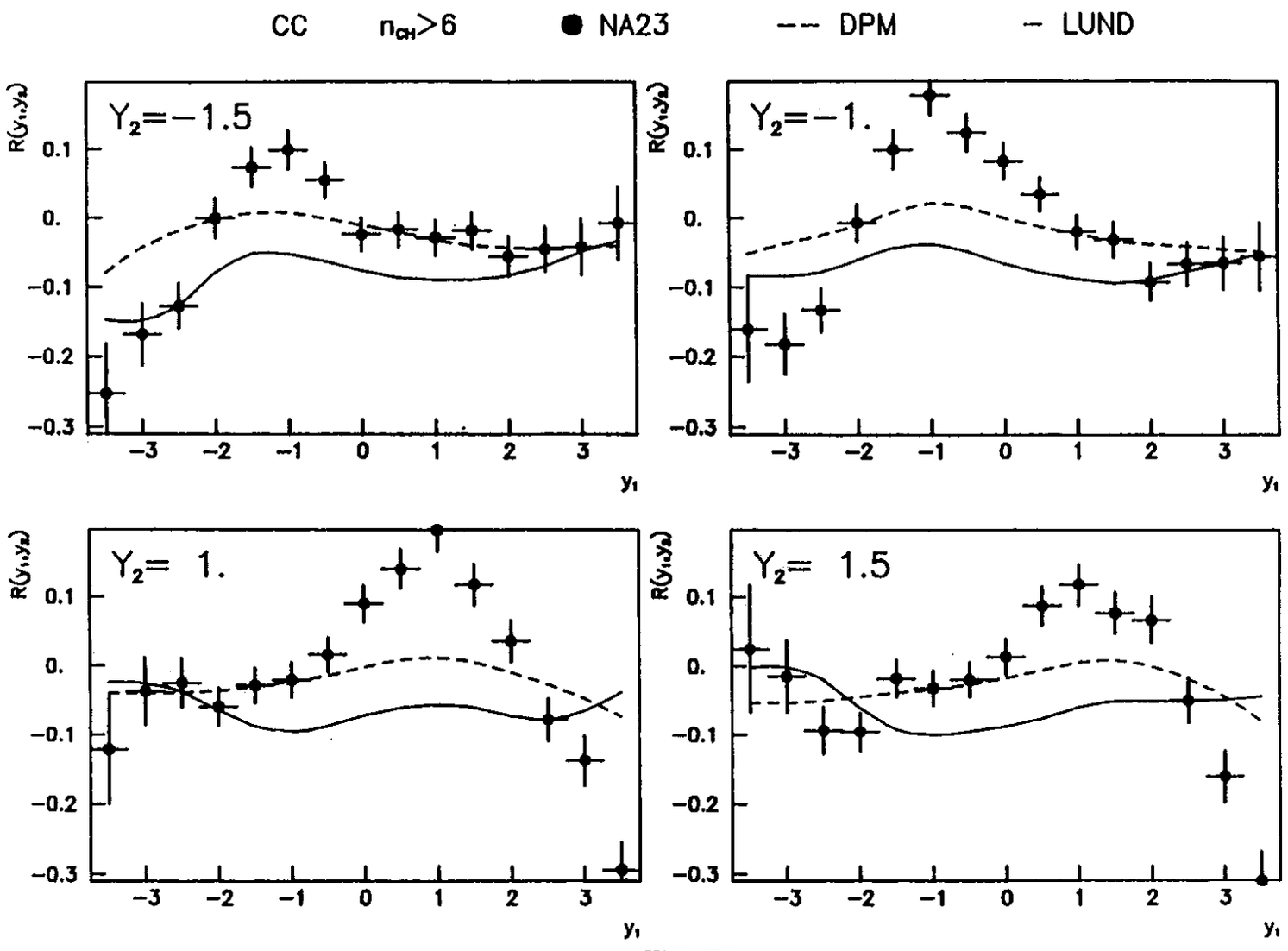
CC $n_{ch}>6$ NA23 DPM LUND
$Y_2=-1.5$
$Y_2=-1.$
$Y_2= 1.$
$Y_2= 1.5$
$R(y_1,y_2)$
$y_1$
0.1
0.
−0.1
−0.2
−0.3
−3
−2
−1
0
1
2
3

FIG.7b

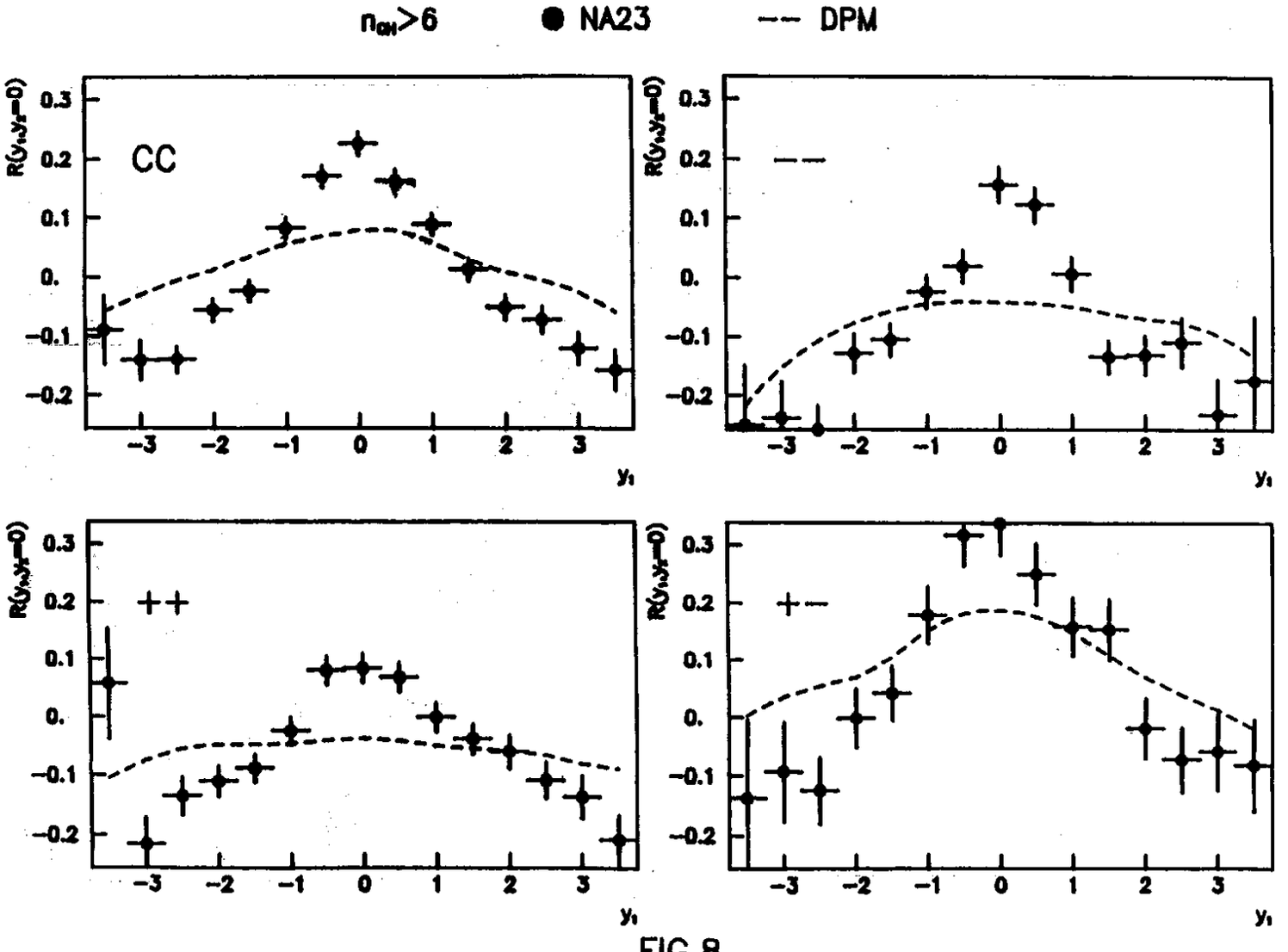


FIG.8

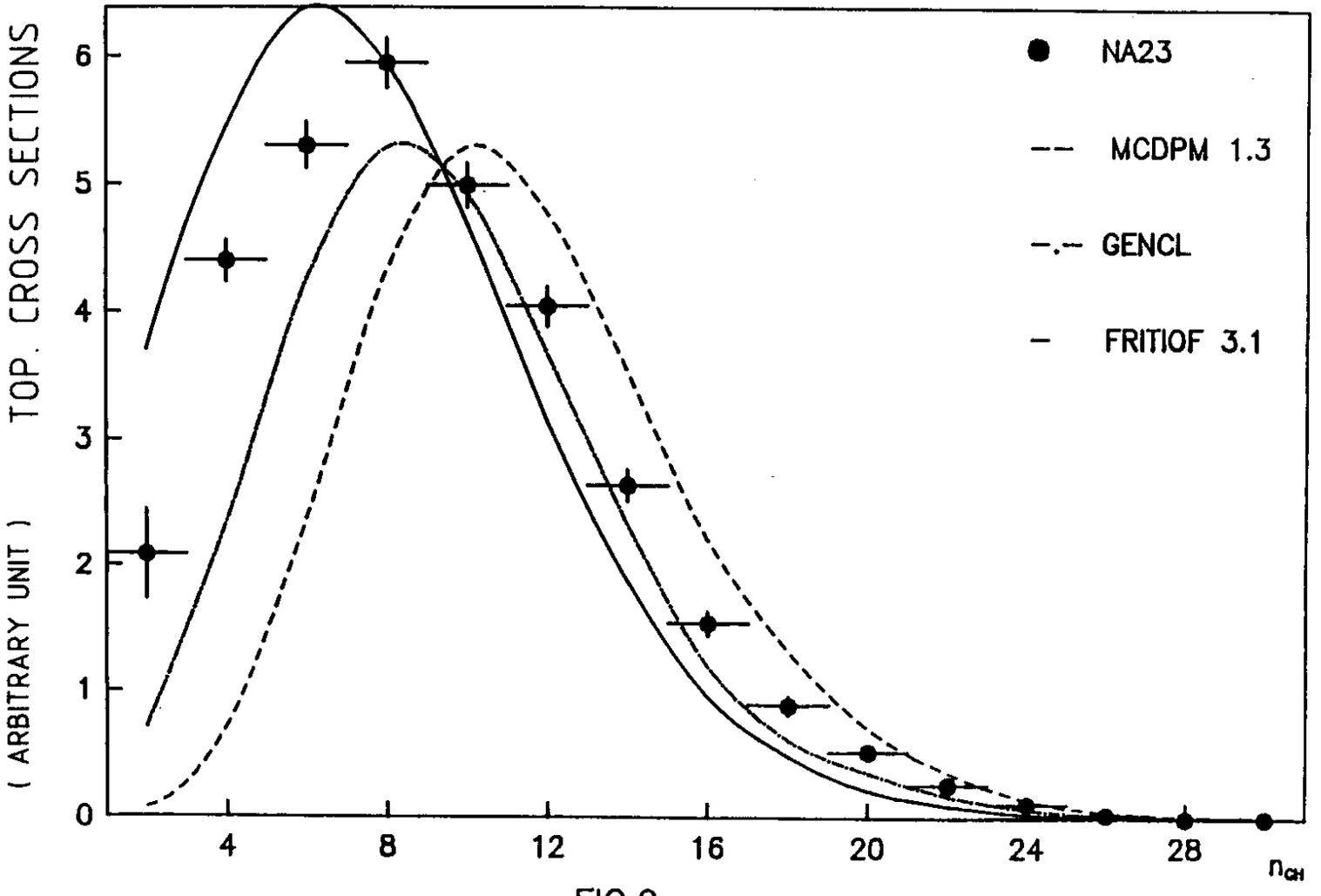
TOP. CROSS SECTIONS
( ARBITRARY UNIT )
0
1
2
3
4
5
6
4
8
12
16
20
24
28
$n_{ch}$
NA23
MCDPM 1.3
GENCL
FRITIOF 3.1

FIG.9

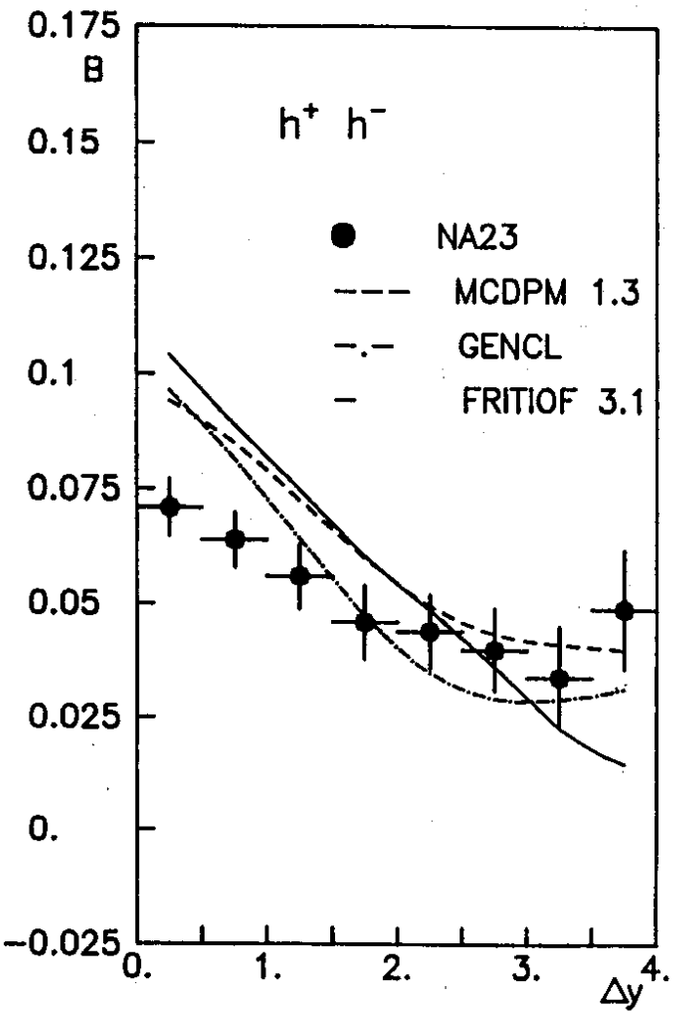
0.175
B
0.15
0.125
0.1
0.075
0.05
0.025
0.
−0.025
0.
1.
2.
3.
4.
Δy
h+ h−
NA23
MCDPM 1.3
GENCL
FRITIOF 3.1

FIG. 10a

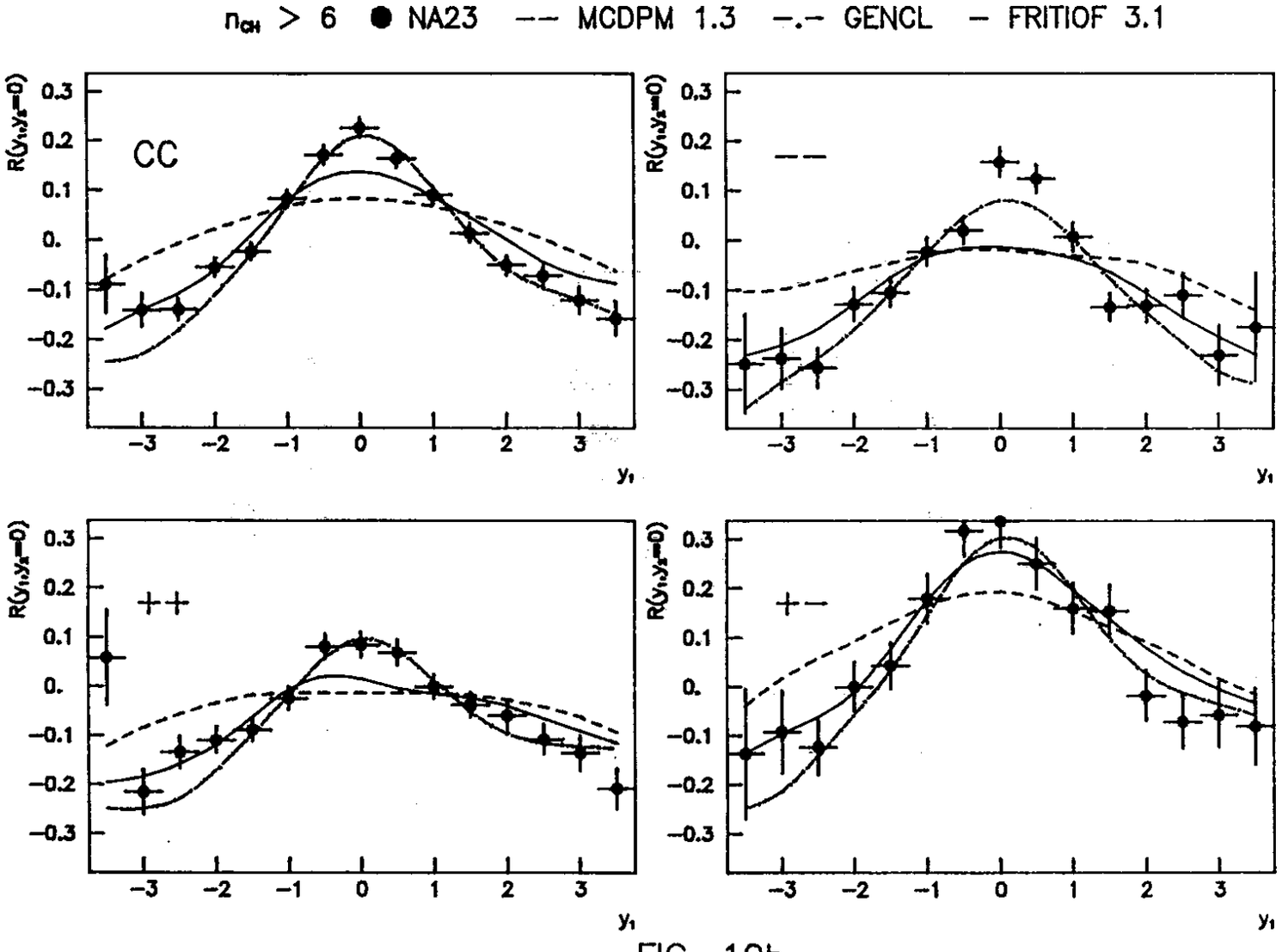


FIG. 10b

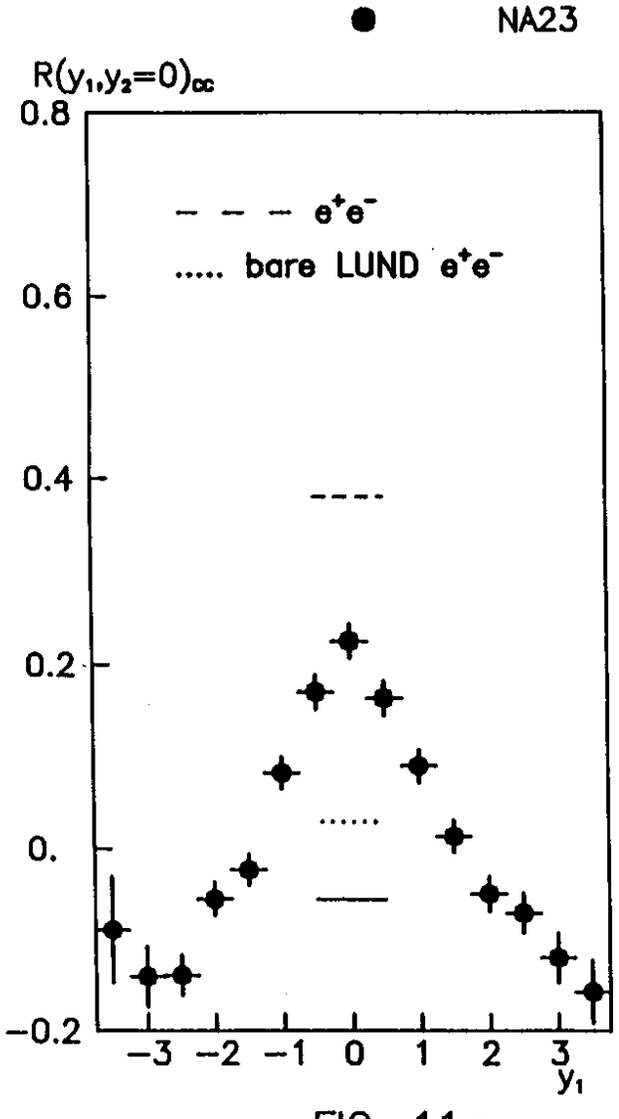


FIG. 11a

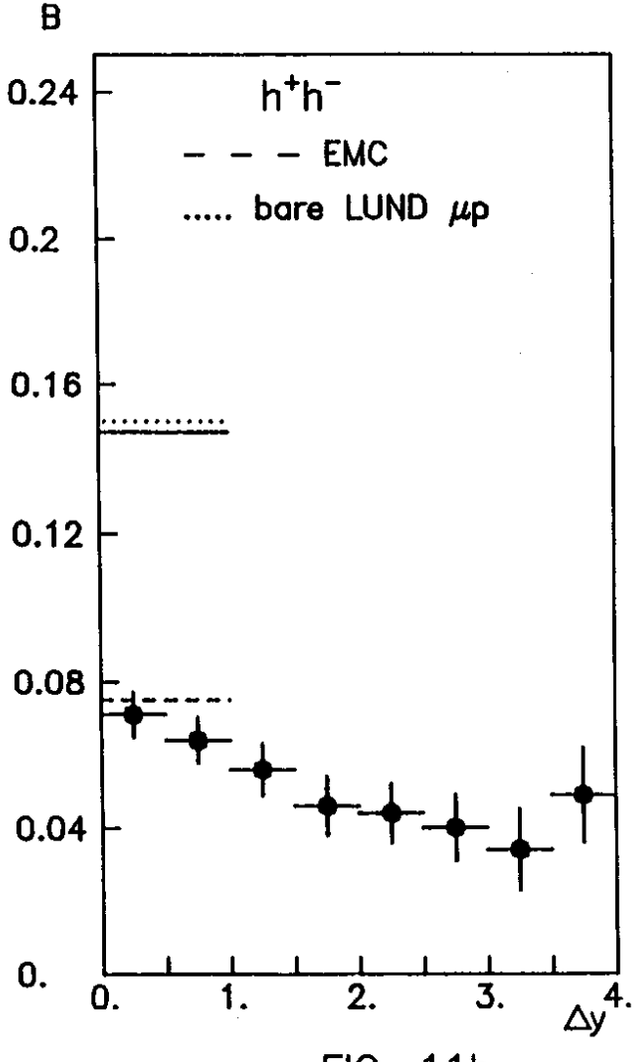


FIG. 11b